Journal of Inflammation Research

Dovepress
open access to scientific and medical research

Open Access Full Text Article

ORIGINAL RESEARCH

Heme-Inducing Endothelial Pyroptosis Plays a Key Role in Radiofrequency Ablation of Hepatic Hemangioma Leading to Systemic Inflammatory Response Syndrome

Changyu Yao*, Jian Kong*, Fei Xu, Shaohong Wang, Shilun Wu, Wenbing Sun, Jun Gao

Department of Hepatobiliary Surgery, Beijing Chaoyang Hospital, Capital Medical University, Beijing, 100043, People's Republic of China

*These authors contributed equally to this work

Correspondence: Wenbing Sun; Jun Gao, Department of Hepatobiliary Surgery, Beijing Chao-Yang Hospital, Capital Medical University, No. 5 Jingyuan Road, Shijingshan District, Beijing, 100043, People's Republic of China, Tel +86-010-51718382, Fax +86-010-51718372, Email sunwenbing@bjcyh.com; gaojun8430@163.com

Journal of Inflammation Research downloaded from https://www.dovepress.com/
For personal use only.

Purpose: Systemic inflammatory response syndrome (SIRS) is a common complication of radiofrequency ablation (RFA) for hepatic hemangiomas. RFA can cause hemolytic reactions during hepatic hemangioma ablation. However, the mechanisms underlying RFA-induced SIRS remain unclear.

Methods: We established an orthotopic liver hemangioma model and performed radiofrequency ablation. The levels of interleukin (IL)-1β and IL-18 and the production of ROS were measured. The wet-to-dry lung ratio, inflammation score, and in vivo endothelial cell permeability were examined. $GSDMD^{-/-}$ mice were used to investigate the effect of heme-inducing SIRS. RNA sequencing (RNA-seq) was performed to identify the main pathways underlying heme-induced SIRS. Western blotting and immunoprecipitation were used to determine the changes and interactions of associated proteins.

Results: The levels of heme, IL-1β, and IL-18 were significantly increased after RFA. The wet-to-dry lung ratio increased in hepatic hemangiomas after RFA, indicating that SIRS occurred. Heme induced increased levels of IL-1β and IL-18, cell death, wet-to-dry lung radio, and inflammation score in vitro and in vivo, indicating that heme induced SIRS and pyroptosis. Furthermore, GSDMD participates in heme-induced SIRS in mice, and GSDMD deletion in mice reverses the effect of heme. Heme regulates NLRP3 activation through the NOX4/ROS/TXNIP-TRX pathway, and an N-acetyl-L-cysteine (NAC) or NOX4 inhibitor (GLX351322) reverses heme-induced SIRS.

Conclusion: Our findings suggest that heme induces endothelial cell pyroptosis and SIRS in mice and decreasing heme levels and ROS scavengers may prevent SIRS in hepatic hemangioma after RFA.

Keywords: hemangioma, radiofrequency ablation, systemic inflammatory response syndrome, pyroptosis, endothelial cells

Introduction

Hepatic hemangiomas are the most prevalent benign tumors of the liver.[1] When the tumor is large (≥5 cm) and the growth trend is pronounced and/or clinical symptoms are present, aggressive treatment is required.[2] Surgical resection is the traditional treatment for hepatic hemangiomas; however, it is traumatic and has many complications.[3] Recently, radiofrequency ablation (RFA) has been increasingly used in the clinical treatment of hepatic hemangiomas, showing advantages such as an obvious curative effect, minimal invasiveness, safety, and good application prospects.

Systemic inflammatory response syndrome (SIRS) is a prevalent complication of hepatic hemangioma after RFA and manifests as changes in body temperature, respiration, heart rate, and white blood cell count during or in the short term.[4] The larger the hepatic hemangioma, the higher the incidence and severity of SIRS. RFA can occasionally cause serious

Received: 12 September 2023
Accepted: 28 December 2023
Published: 18 January 2024

© 2024 Yao et al. This work is published and licensed by Dove Medical Press Limited. The full terms of this license are available at https://www.dovepress.com/terms.php and incorporate the Creative Commons Attribution – Non Commercial (unported, v3.0) License (http://creativecommons.org/licenses/by-nc/3.0/). By accessing the work you hereby accept the Terms. Non-commercial uses of the work are permitted without any further permission from Dove Medical Press Limited, provided the work is properly attributed. For permission for commercial use of this work, please see paragraphs 4.2 and 5 of our Terms (https://www.dovepress.com/terms.php).

Graphical Abstract

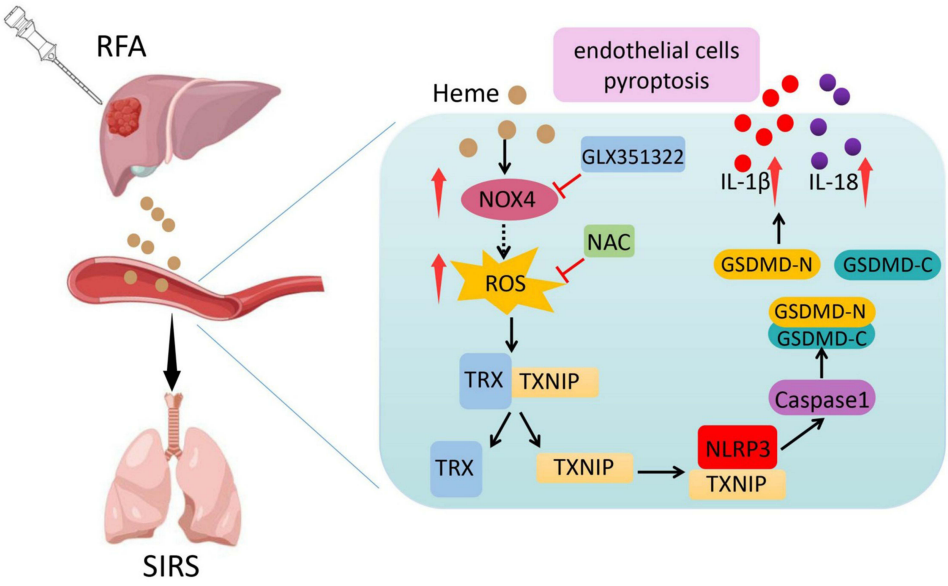

complications, such as acute respiratory distress syndrome (ARDS) and myocardial injury.[5,6] However, the mechanisms underlying RFA-induced SIRS remain unclear.

RFA can lead to hemolytic reactions during hepatic hemangioma ablation, and damaged red blood cells release hemoglobin into the bloodstream, which is then broken down into heme and globin. Heme, a typical damage-associated molecular pattern (DAMP), recognizes receptors through patterns such as Toll-like receptors, induces autoimmune or immune tolerance, and plays an important role in the development of inflammation.[7–10] Heme can induce lipid peroxidation and mediate TNF-α-mediated programmed cell death.[11] In endothelial cells, heme not only activates NLRP3 inflammatory bodies, leading to inflammation but also induces endothelial barrier disturbance through the MKK3/p38MAPK axis, leading to impaired lung function.[12,13] Therefore, heme may participate in the SIRS of hepatic hemangiomas after RFA.

Pyroptosis is a programmed cell death that manifests itself in cell swelling until the cell membrane ruptures, releasing cell contents, interleukin (IL)-1β, and IL-18, which activate inflammation.[14–16] Wu et al reported that caspase-4/11-mediated pulmonary artery endothelial cell scorching death led to the development of pulmonary hypertension.[17] Kerr et al reported that in traumatic brain injury, extracellular vesicles in the serum can stimulate the death of human lung microvascular endothelial cells, leading to lung damage.[18] Jia et al found that a possible pathophysiological mechanism of Kawasaki disease is that the HMGB1/NLRP3/caspase-1 signaling pathway induces endothelial cell scorching, which in turn leads to coronary artery damage.[19] Our previous study showed that endothelial pyroptosis might be involved in the occurrence of SIRS.[20,21] However, the mechanisms underlying heme-induced SIRS in hepatic hemangiomas after RFA remain unknown.

In this study, we showed that heme levels increased and SIRS was induced in an orthotopic transplantation model of hepatic hemangioma after RFA. Heme-induced endothelial pyroptosis through the NOX4/ROS/NLRP3 pathway in hepatic hemangioma after RFA, and N-acetyl-L-cysteine (NAC) or a NOX4 inhibitor (GLX351322) reversed heme-induced SIRS. Our findings provide an explanation for the mechanisms and potential targets of SIRS in hepatic hemangiomas following RFA.

Materials and Methods

Cell Culture

Human lung microvascular endothelial cells (HLMVECs) were purchased from Wuhan Procell Life Science and Technology Company (CP-H001) and cultured in complete ECM medium (Science, Carlsbad, CA, USA) supplemented with 1% ECGS, 100 U/mL penicillin/streptomycin, 5% FBS, and 100 μg/mL streptomycin in a humidified incubator at 37°C with 5% CO_2. For the heme stimulation experiment, HLMVECs were treated with heme (40 μM) for 24 h. Cell lysates and cell culture medium were collected for subsequent experiments.

Heme Measurement

Serum heme levels were measured using an Abcam Hemin assay kit (ab65332) according to the manufacturer's protocols.

Transfection Experiments

Lentivirus-mediated shRNA NLRP3, shRNA NOX4, and shRNA TXNIP were purchased from GeneChem (Shanghai, China). HLMVECs were seeded in the complete ECM medium and transfected with lentivirus at 50%–60% confluency of cells according to the manufacturer's protocols. An empty vector was used as a negative control. The ECM medium was replaced with fresh ECM after 12 h. The expression of green fluorescent protein was detected by fluorescence microscopy three days later. Transfected HLMVECs were collected for subsequent culturing. Targeted genes that were knocked down were analyzed by Western blotting. Target sequences were shown as follows:

sh-NLRP3:5′-GGAGAGACCTTTATGAGAAAG-3′;
sh-NOX4: 5′-GAGCCTCAGCATCTGTTCTTA-3′;
sh-TXNIP: 5′-GGCAATCTCCTGGGCCTTAAA-3′.

Western Blot Analysis

The HLMVECs were lysed in radioimmunoprecipitation assay lysis buffer containing protease and phosphatase inhibitors (Solarbio). Protein concentration in the cell lysate was determined using a bicinchoninic acid (BCA) protein quantification kit. Protein samples were separated using sodium dodecyl sulfate–polyacrylamide gel electrophoresis and transferred onto a nitrocellulose membrane. The membrane was blocked with 5% non-fat milk for 1 h and incubated with primary antibody at 4 °C overnight. Primary antibodies used in this assay were as follows: GSDMD (Abcam, ab210070), GSDMD-N (Abcam, ab215203), Caspase1 (Abcam, ab207802), Caspase1 p20 (CST, 4199T), IL-1β (CST, 83186), IL-18 (Abcam, ab243091), NLRP3 (Abcam, ab263899), NOX4 (Abcam, ab133303), TRX (abcam, ab133524), TXNIP (CST, 14715). Protein signals were detected using SuperSignal West Pico substrate (Thermo Scientific, Rockford, IL, USA). Finally, the protein signals were quantified by ImageJ.

ELISA

The levels of IL-1β (Abcam, ab197742) and IL-18 (R&D, DY7625) were quantified in mouse plasma samples. The levels of IL-1β (Abcam, ab100562) and IL-18 (NOVUS, KA0561) of HLMVECs conditioned medium were quantified using ELISA kits according to the manufacturer's instructions.

In vitro Permeability Assay

An in vitro permeability assay was performed as described previously. Briefly, HLMVECs (1×10^5) were cultured in collagen-coated transwell inserts (Corning, Corning, NY, USA) to form a monolayer. Subsequently, 70 KDa (250 μg mL^{-1}) tetramethylrhodamine-dextran (Invitrogen, Carlsbad, CA, USA) was added to the transwell insert. The medium was removed from the lower compartment at 10, 20, 60, and 90 min. The permeability rate was determined by measuring the tetramethylrhodamine-dextran fluorescence intensity of the medium in the lower compartment using a NOVOstar microplate reader (BMG Labtech, Ortenberg, Germany).

Murine Hepatic Hemangioma Model and RFA in vivo

Of note, 30 μL of suspension containing H5V endothelial cells (5×10^6) and Matrigel was injected into the subcapsular region of the liver parenchyma in the median lobe. The tumor volume was measured at the indicated time until it reached a length of approximately 1 cm, and RFA was performed. A radiofrequency current generator (Covidien, Mansfield, MA, USA) was used to generate radiofrequency energy. A 17-gauge cool-tip electrode of 15 cm length with 0.7 cm exposed tip (Covidien, Mansfield, MA, USA) was used to deliver the radiofrequency energy. Each ablation cycle lasted 5 s.

Animal Experiment

The animals used in this study were pathogen-free mice aged 8–12 weeks. The mice were randomly assigned to each group. Heme (Sigma-Aldrich, St. Louis, MO, USA) was injected intraperitoneally at a dose of 20 μM/kg body weight. In one experiment, we injected C57BL/6 mice with heme, and the control mice received PBS only. In another experiment, mice were pretreated with NAC (300 mg/kg/day) or GLX351322 (4 mg/kg/day) and heme was injected intraperitoneally. Plasma and lungs were collected from mice 24 h after heme treatment. For gene-knockout animals, $GSDMD^{-/-}$ and WT mice were assigned to each group and injected with heme. Plasma and lungs were collected from the mice 24 h after heme treatment.

Inflammation Score

The inflammation score was calculated as described before.[22] Symptoms, including periorbital exudates, tremors, lethargy, respiratory distress, diarrhea, and piloerection, were observed after heme injection. The presence of each condition was scored as 1 or 2.

Detection of Cell Death

After different stimulations of HLMVECs, PI (2 μg/ mL) and Hoechst (5 μg/ mL) were added into the cell culture medium and incubated for 10 min at room temperature. Cell images were obtained at random using a fluorescent cell imager.

To analyze cell death, LDH release was detected using an LDH cytotoxicity assay kit according to the manufacturer's instructions. Of note, 120 μL of cell supernatant and 60 μL of prepared LDH reagent were added to the 96-well plate, and incubated on a horizontal shaker for 30 minutes in the dark. The absorbance of the samples was measured at 490 nm using a NOVOstar Microplate Reader.

Detection of ROS

The DCFH-DA fluorescent probe was used to measure the intracellular ROS levels in HLMVECs. Heme-incubated cells were then incubated with DCFH-DA (10 μM) for 30 min in the dark. Cell images were obtained at random using a fluorescent cell imager.

In vivo Assessment of Vascular Permeability

The mice were injected with heme, and 12 h later, multiphoton imaging was performed as previously described. Briefly, tetramethylrhodamine-dextran (40 KDa, 0.1 mL of 10 mg/ mL) was injected into the tail vein. The mice were sacrificed and the lungs were surgically exposed and removed to prepare frozen sections 10 min later. The relative fluorescence intensity around the vessel was measured using the ImageJ software (NIH).

Immunoprecipitation

HLMVECs were lysed in radioimmunoprecipitation assay lysis buffer containing protease and phosphatase inhibitors. The supernatant was collected after centrifugation of the lysate at 13,000 g for 10 min. Of note, 2 μL primary antibody and 100 μL protein Agarose beads were added to the supernatant at 4 °C for 4 h. Primary antibodies were as follows: anti-TRX (Abcam, ab133524), anti-TXNIP (CST, #14715) and anti-NLRP3 (Abcam, ab263899). The immunocomplexes were washed in 250 μL NaCl four times and then subjected to to Western blot. The protein signals were quantified by ImageJ.

RNA-Seq Analysis

The corresponding testing methods for quality inspection according to the requirements of samples and products are selected. A certain amount of RNA samples are denatured at suitable temperature to open their secondary structure, and mRNA is enriched by oligo (dT) -attached magnetic beads. The reaction system is configured. After reacting at the suitable temperature for a fixed period of time, RNAs are fragmented. The first-strand synthesis reaction system is prepared, and the reaction program, synthesize the first- strand cDNA are set up. The the second-strand synthesis reaction system is prepared, and the reaction program to synthesize the second-strand cDNA is set up. After the reaction system and program are configured and set up, double-stranded cDNA fragments are subjected to end-repair, and then a single "A" nucleotide is added to the 3' ends of the blunt fragments. The reaction system and program for adaptor ligation are subsequently configured and set up to ligate adaptors with the cDNAs. The PCR reaction system and program are configured and set up to amplify the product. The corresponding library quality control protocol is selected depending upon product requirements. Single-stranded PCR products are produced via denaturation. The reaction system and program for circularization are subsequently configured and set up. Single-stranded cyclized products are produced, while uncyclized linear DNA molecules are digested. Single-stranded circle DNA molecules are replicated via rolling cycle amplification, and a DNA nanoball (DNB) which contain multiple copies of DNA is generated. Sufficient quality DNBs are then loaded into patterned nanoarrays using high-intensity DNA nanochip technique and sequenced through combinatorial Probe-Anchor Synthesis (cPAS). The raw paired-end reads were trimmed and quality controlled by SeqPrep (https://github.com/jstjohn/SeqPrep) and Sickle (https://github.com/najoshi/sickle) with default parameters. Clean reads were separately aligned to the reference genome with orientation mode using HIASAT (https://ccb.jhu.edu/software/hisat2/index.shtml) software. The mapped reads of each sample were assembled by StringTie (https://ccb.jhu.edu/software/stringtie/ index.shtml=example) using a reference-based approach. To identify DEGs (differential expression genes) between different samples, the expression level of each transcript was calculated according to the Transcripts Per Million reads (TPM) method. RSEM (http://deweylab. biostat.wisc.edu/rsem/) was used to quantify gene abundances. Rstatistical package software DESeq2 (http://bioconductor.org/packages/stats/bioc/DESeq2/) was utilized for differential expression analysis.

Real-Time PCR

Total RNA was extracted using the TRIzol reagent (Invitrogen, Carlsbad, CA, USA). RNA was reverse transcribed to obtain cDNA using the SuperScript III First-Strand Synthesis Kit (Invitrogen). cDNA was amplified using SYBR Green PCR Master Mix (Applied Biosystems) for real-time PCR analyses in a Bio-Rad C1000 Thermal Cycler. The relative RNA expression levels were calculated using the -ΔΔCT method. The primers used in this study were as follows: NOX4: GCAGGAGAACCAGGAGATTG (forward), CACTGAGAAGTTGAGGGCATT (reverse); GAPDH: TGTGGGCATCAATGGATTTGG (forward), ACACCATGTATTCCGGGTCAAT (reverse).

Wet-to-Dry Lung Ratio

The isolated lungs were weighed (wet weight). Then, the lungs were dried in an oven at 60°C for 48 h and weighed (dry weight). Wet and dry weights were measured to calculate the wet-to-dry lung ratio.

Statistical Analysis

The statistical data were expressed as the mean ± SEM. A two-tailed Student's *t*-test or one-way ANOVA variance was used to calculate statistically significant differences. Statistical significance was set at $P < 0.05$. All statistical analyses were performed using GraphPad Prism version 8.

Results

SIRS Occurred in Hepatic Hemangioma After RFA and Heme Level Was Increased

We established an orthotopic liver hemangioma model and performed RFA to simulate human hemangioma ablation (Figure 1a). CD31 immunohistochemical staining was performed to verify the establishment of orthotopic liver

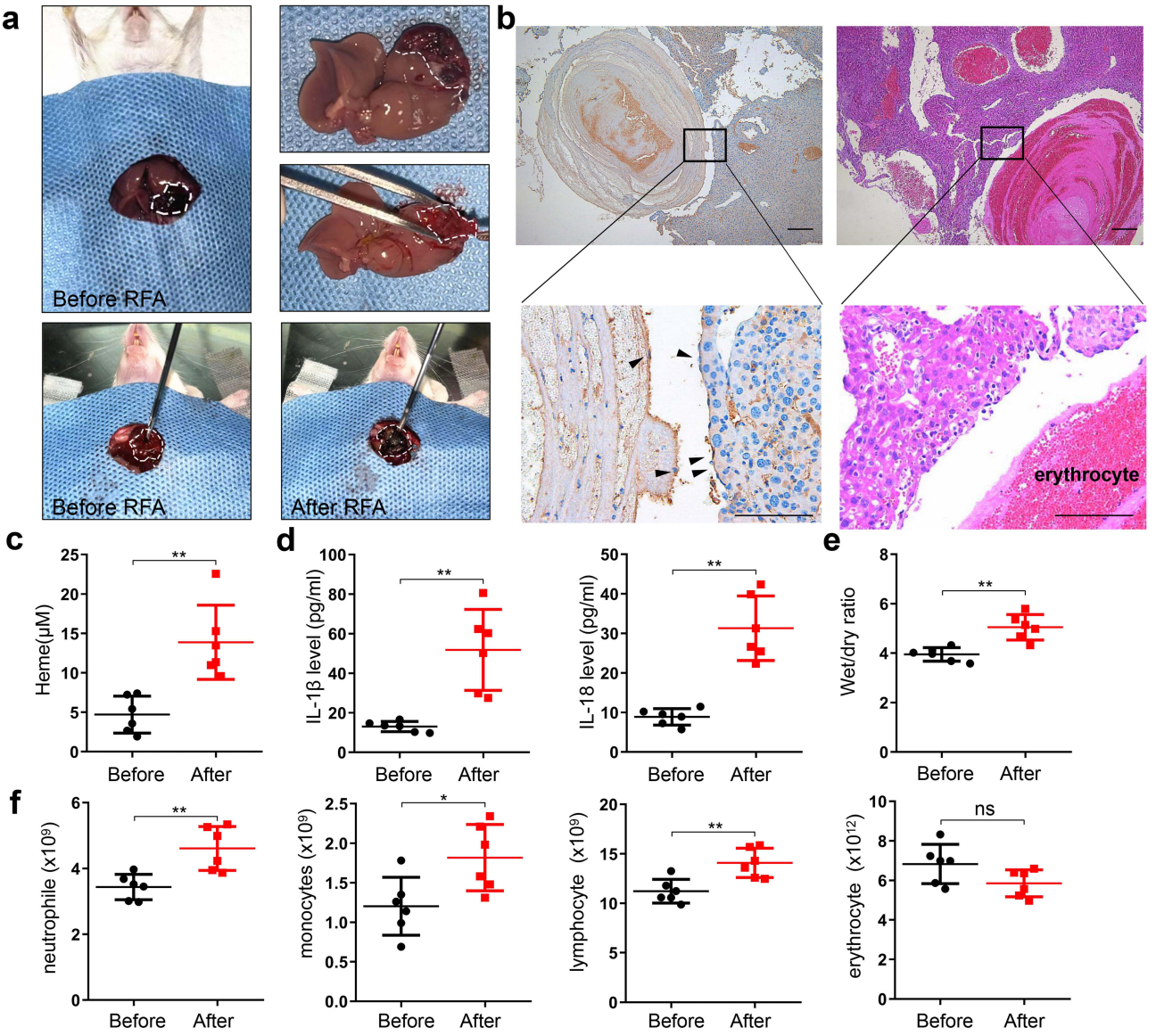

Figure 1 SIRS occurred and heme elevated after RFA of hepatic hemangioma in mice. (**a**) The orthotopic liver hemangioma model was established, and RFA was performed. (**b**) The liver hemangioma of mice was stained by CD31 immunohistochemical staining and H&E staining, black arrow indicates the positive CD31 staining. Scale bar = 200 μm. (**c**) The level of heme in mice was detected after RFA. (**d**) The levels of IL-1β and IL-18 were detected by ELISA. (**e**) The wet-to-dry lung ratio was calculated. (**f**) The neutrophil, monocyte, lymphocyte, and erythrocyte count were examined. There were 6 mice in each group. The data are expressed as mean ± SEM. ns: no significance, *P < 0.05, **P < 0.01.

hemangioma. The results showed that CD31 staining was positive in the capsule of the hepatic tumor, demonstrating that the hepatic hemangioma model was successfully established (Figure 1b). Furthermore, serum heme elevated in mice with hemangioma compared to that in control liver after RFA, indicating that heme could derive from ablated hemangioma tissue (Supplemental Figure 1a). The levels of heme, IL-1β, and IL-18 in serum were significantly increased at 24 h after RFA compared with that before RFA (Figure 1c and d).The wet-to-dry lung ratio increased after RFA (Figure 1e), and the neutrophil, monocyte, and lymphocyte counts also significantly increased after RFA, indicating that SIRS occurred after RFA for hepatic hemangioma (Figure 1f). Taken together, these findings demonstrate that SIRS occurs in hepatic hemangiomas following RFA.

Heme Induces SIRS in Mice

To determine the effect of heme on SIRS, heme was injected into mice. The levels of IL-1β and IL-18 in serum were significantly increased in mice after the treatment of heme (Figure 2a). The wet-to-dry lung ratio increased after heme

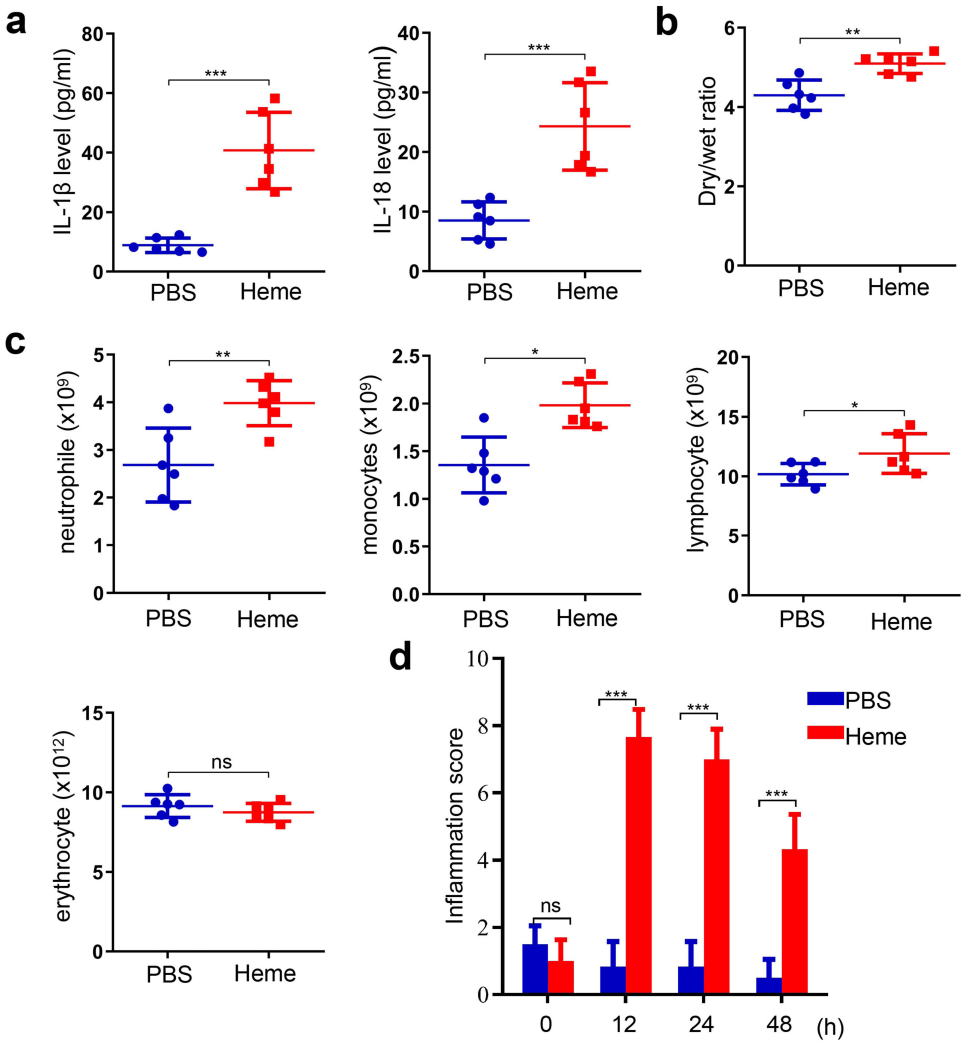

Figure 2 Heme induces SIRS in mice. (**a**) The levels of IL-1β and IL-18 were detected after heme treatment. (**b**) The wet-to-dry lung ratio was calculated after heme treatment. (**c**) The neutrophil, monocyte, erythrocyte, and lymphocyte count were detected. (**d**) The inflammation score of mice was measured at 0 h, 12 h, 24 h, and 48 h after heme treatment. There were 6 mice in each group. The data are expressed as mean ± SEM. ns: no significance, *P < 0.05, **P < 0.01, ***P < 0.001.

treatment (Figure 2b). Furthermore, the neutrophil, monocyte, and lymphocyte counts significantly increased after heme treatment (Figure 2c). In addition, the inflammation score of the mice were recorded at 0, 12, 24, and 48 h to evaluate the SIRS. The results showed that the inflammation score significantly increased at 12 and 24 h and slightly decreased at 48 h (Figure 2d). Taken together, these results indicated that heme induces SIRS in mice.

NLPR3 is Involved in Heme-Leading SIRS

Previous studies have demonstrated that heme may induce inflammation of endothelial cells.[23] To investigate whether heme can cause SIRS by inducing endothelial cell inflammation, human lung microvascular endothelial cells (HLMVECs) were treated with heme. Heme induced morphological changes in cells after heme treatment (Figure 3a). The PI staining results indicated that more HLMVECs died after heme treatment (Figure 3b) and LDH release increased after heme treatment (Figure 3c). The levels of IL-1β and IL-18 in conditioned media collected from HLMVECs were also increased after heme treatment (Figure 3d). Activation of the NLRP3 inflammasome and pyroptosis promote inflammation. To investigate the effect of NLRP3 on heme-induced SIRS, heme were treated with HLMVECs. Western blot results showed that IL-1β and IL-18 were increased in HLMVECs after heme treatment (Figure 3e). Meanwhile, NLRP3 knockdown downregulated the expression of IL-1β and IL-18 in HLMVECs, which reversed the effect of heme (Figure 3f). NLPR3 downregulation also reversed the elevated levels of IL-1β and IL-18 in conditioned

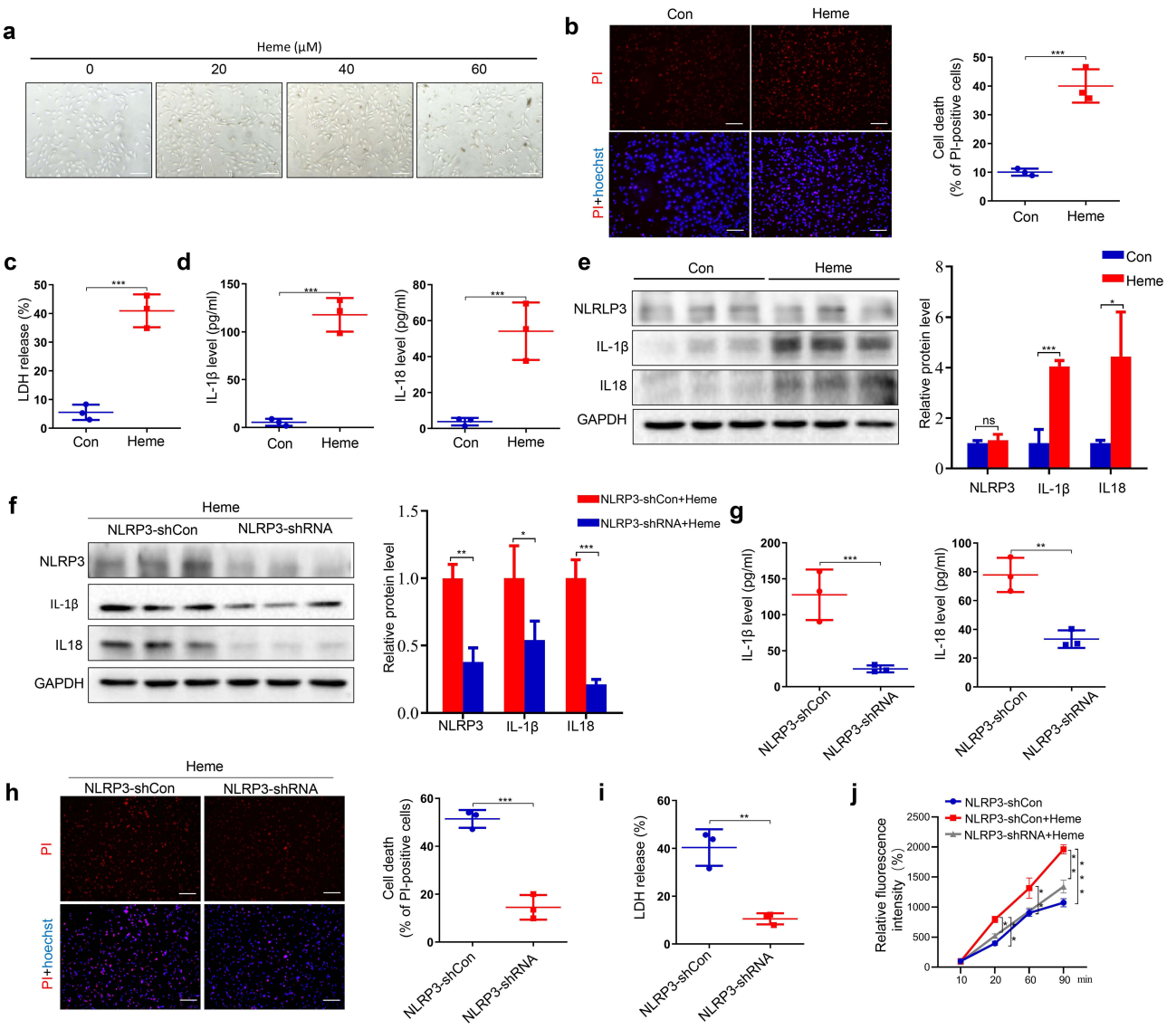

Figure 3 NLPR3 participates in heme-inducing SIRS. (**a**) The morphological change of HLMVECs was observed at 24 h after heme treatment. Scale bar = 100 μm. (**b**) The HLMVECs were stained with PI and Hoechst for 20 min after heme treatment at 24 h. Scale bar = 50 μm. (**c**) Analysis of culture supernatant LDH levels of HLMVECs after heme treatment. (**d**) The levels of IL-1β and IL-18 in HLMVECs media were measured by ELISA after heme treatment. (**e**) The expression of NLRP3, IL-1β, and IL-18 in HLMVECs was assayed by Western blotting after heme treatment. (**f**) The expression of NLRP3, IL-1β, and IL-18 in HLMVECs with knocked-down NLPR3 were assayed by Western blotting after heme treatment. (**g**) The levels of IL-1β and IL-18 in HLMVECs with knocked-down NLPR3 media were measured by ELISA after heme treatment. (**h**) The HLMVECs were stained with PI and Hoechst for 20 min in HLMVECs with knocked-down NLPR3 after heme treatment at 24 h. Scale bar = 100 μm. (**i**) Analysis of culture supernatant levels of LDH in HLMVECs with knocked-down NLPR3 after heme treatment. (**j**) Media from the lower chamber of HLMVECs was taken to measure fluorescence intensities at 10 min, 20 min, 60 min, and 90 min after heme treatment. The data are expressed as mean ± SEM. ns: no significance, *P < 0.05, **P < 0.01, ***P < 0.001.

media from HLMVECs after heme treatment (Figure 3g). Furthermore, PI staining results showed that NLRP3 knockdown suppressed the death of HLMVECs (Figure 3h), and LDH release decreased in NLRP3 knockdown HLMVECs after heme treatment, indicating that NLPR3 may be involved in heme-induced pyroptosis (Figure 3i). An endothelial permeability assay was performed to evaluate SIRS-inducing leakage of vessels in vitro. Pretreatment with heme allowed more dextran to traverse the endothelial monolayer of HLMVECs, and knocking down NLRP3 rescued this effect, indicating that heme promotes endothelial permeability through NLRP3 in SIRS (Figure 3j).

GSDMD Participates in the Heme-Inducing SIRS in Mice

Given that GSDMD is an executor of pyroptosis and is activated by the NLRP3 inflammasome, we investigated the effect of GSDMD on heme-induced SIRS. Knockdown of NLPR3 in HLMVECs suppressed the heme-induced increase in the abundance of Casp1 p20 and GSDMD-N (Figure 4a). Next, we used GSDMD$^{-/-}$ and wild-type mice to investigate the

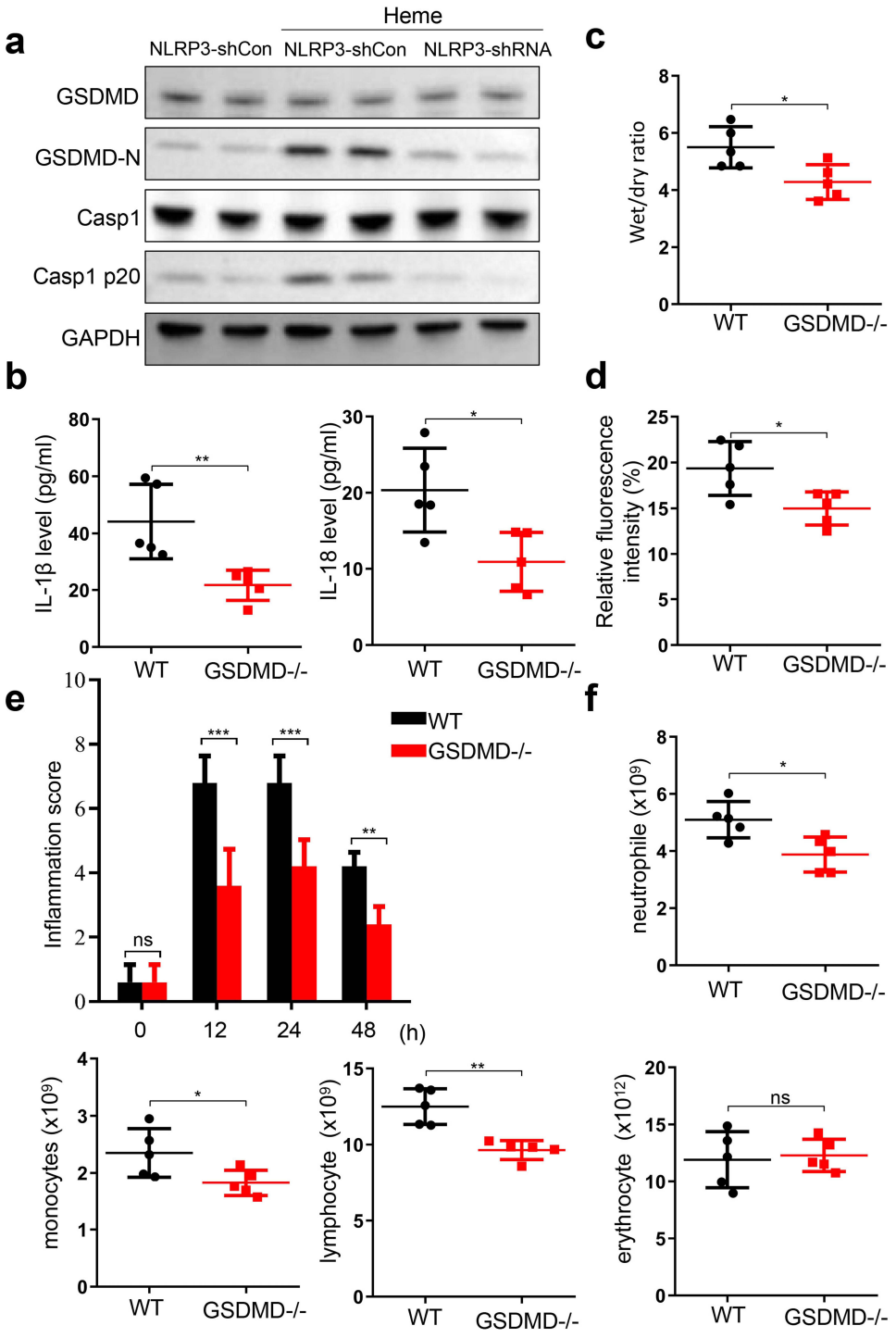

Figure 4 GSDMD is involved in the heme-inducing SIRS in mice. (**a**) The expression of GSDMD, GSDMD-N, Casp1, and Casp1 p20 in HLMVECs after NLRP3 knockdown were assayed by Western blotting after heme treatment. (**b**) The levels of IL-1β and IL-18 in WT and GSDMD$^{-/-}$ mice serum were detected after heme treatment. (**c**) The wet-to-dry lung ratio in WT and GSDMD$^{-/-}$ mice was calculated after heme treatment. (**d**) WT and GSDMD$^{-/-}$ mice were intravenously injected with tetramethylrhodamine-dextran after heme treatment at 24 h and the lung vascular permeability was examined by multiphoton-microscope. (**e**) The inflammation score of WT and GSDMD$^{-/-}$ mice was measured at 0 h, 12 h, 24 h, and 48 h after heme treatment. (**f**) The neutrophil, monocyte, erythrocyte, and lymphocyte count in WT and GSDMD$^{-/-}$ mice were detected after heme treatment. There were 5 mice in each group. The data are expressed as mean ± SEM. ns: no significance, *P < 0.05, **P < 0.01, ***P < 0.001.

effect of GSDMD on heme-induced SIRS. The serum levels of IL-1β and IL-18 in GSDMD$^{-/-}$ mice after heme treatment were significantly decreased compared with that in wild-type mice (Figure 4b). The wet-to-dry lung ratio also decreased after heme treatment in GSDMD$^{-/-}$ mice (Figure 4c). More severe vascular permeability was observed in wild-type mice after heme treatment than in GSDMD$^{-/-}$ mice (Figure 4d). Furthermore, the inflammation scores significantly decreased

at 12, 24, and 48 h in GSDMD$^{-/-}$ mice after heme treatment (Figure 4e). Neutrophil, monocyte, and lymphocyte counts significantly decreased in GSDMD$^{-/-}$ mice after heme treatment (Figure 4f).

Heme Regulates NLRP3 Activation Through NOX4/ROS/TXNIP/TRX Pathway

Since heme did not regulate NLRP3 expression (Figure 3e), we investigated the mechanism by which heme regulated NLRP3 activation. RNA-seq analysis was used to examine the mRNA changes in HLMVECs with or without heme treatment. mRNAs with fold changes ≥1.5 and P-value<0.05 were identified as differentially expressed mRNAs. NOX4 was one of upregulated genes, and the mRNA and protein expression of NOX4 were upregulated in HLMVECs after heme treatment (Figure 5a and b). Previous studies have shown that NADPH oxidases (NOXs) are the main enzymes involved in ROS production;[24] therefore, we measured ROS expression in HLMVECs. Our data showed that heme promoted ROS generation in HLMVECs and NOX4 knockdown suppressed heme-induced ROS generation (Figure 5c and d). Given that excessive ROS can regulate TXNIP binding of TXNIP to NLRP3 and activate the NLRP3 inflammasome in macrophages, we investigated whether NOX4 regulates the NLRP3 inflammasome via the ROS/TXNIP/TRX pathway in HLMVECs. Western blot results showed that NOX4 knockdown did not influence the expression of TXNIP and TRX (Figure 5e), indicating that NOX4 may regulate the interaction between TXNIP and TRX. The immunoprecipitation results showed that NOX4 knockdown significantly promoted the interaction between TXNIP and TRX (Figure 5f). The NOX4 knockdown suppressed the interaction between TXNIP and NLRP3 (Figure 5f). Furthermore, TXNIP knockdown inhibited the heme-induced increase in the levels of GSDMD-N and Casp1 p20 (Figure 5g). Overall, the results indicate that NOX4 upregulation promotes the dissociation of TXNIP and TRX through ROS and that free TXNIP interacts with NLPR3 and promotes NLPR3 activation, inducing an increased abundance of GSDMD-N and Casp1 p20.

NAC and GLX351322 Reverse Heme-Inducing SIRS

NAC was used to examine the effects of heme-induced SIRS in mice. The serum levels of IL-1β and IL-18 in mice after heme and NAC treatment were significantly decreased compared with that in heme treatment (Figure 6a). Vascular

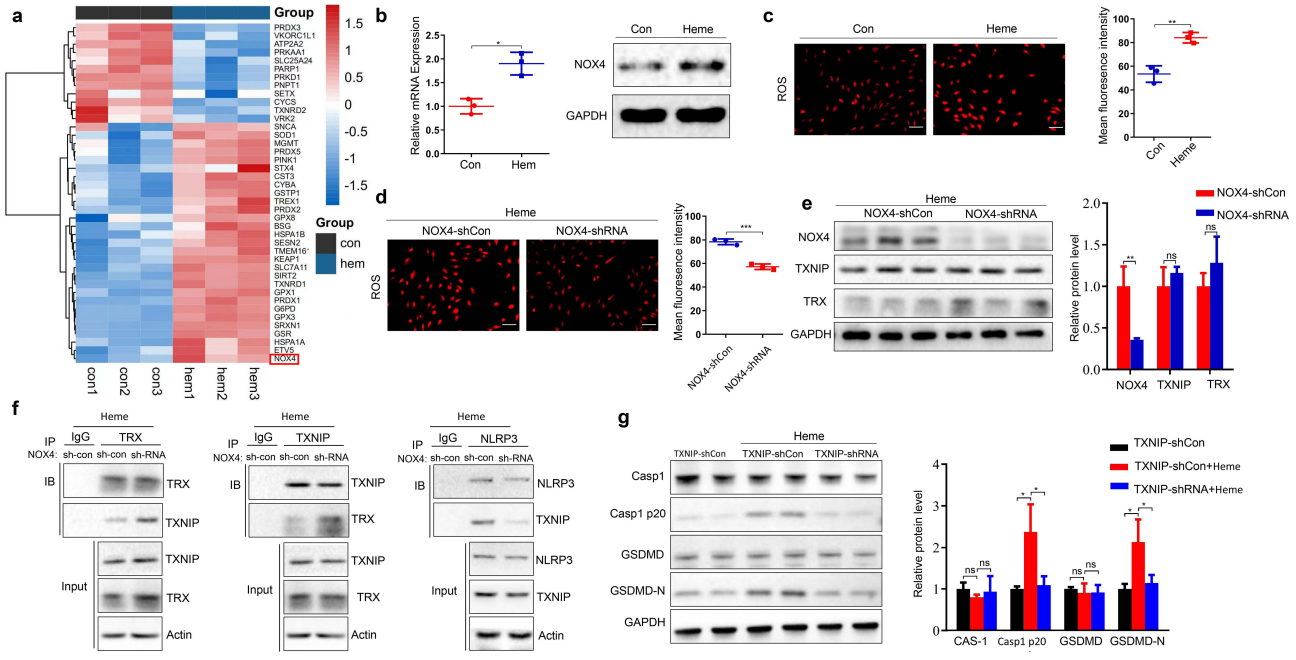

Figure 5 NOX4 regulates NLRP3 activity through TXNIP/TRX. (**a**) Representative heat map of differentially expressed genes in HLMVECs after heme treatment. (**b**) The mRNA and protein of NOX4 in HLMVECs were detected after heme treatment. (**c**) The ROS content in HLMVECs was assayed after heme treatment. Scale bar = 100 μm. (**d**) The ROS content in HLMVECs with knocked-down NOX4 was assayed after heme treatment. Scale bar = 100 μm. (**e**) The expression of NOX4, TXNIP, and TRX in HLMVECs with knocked-down NOX4 was detected by Western blotting after heme treatment. (**f**) Interactions of endogenous TRX, TXNIP, and NLRP3 were determined by immunoprecipitation analyses in HLMVECs with knocked-down NOX4 after heme treatment. (**g**) The expression of GSDMD, GSDMD-N, Casp1, and Casp1 p20 in HLMVECs with knocked-down TXNIP was detected by Western blotting after heme treatment. The data are expressed as mean ± SEM. ns: no significance, *P < 0.05, **P < 0.01, ***P < 0.001.

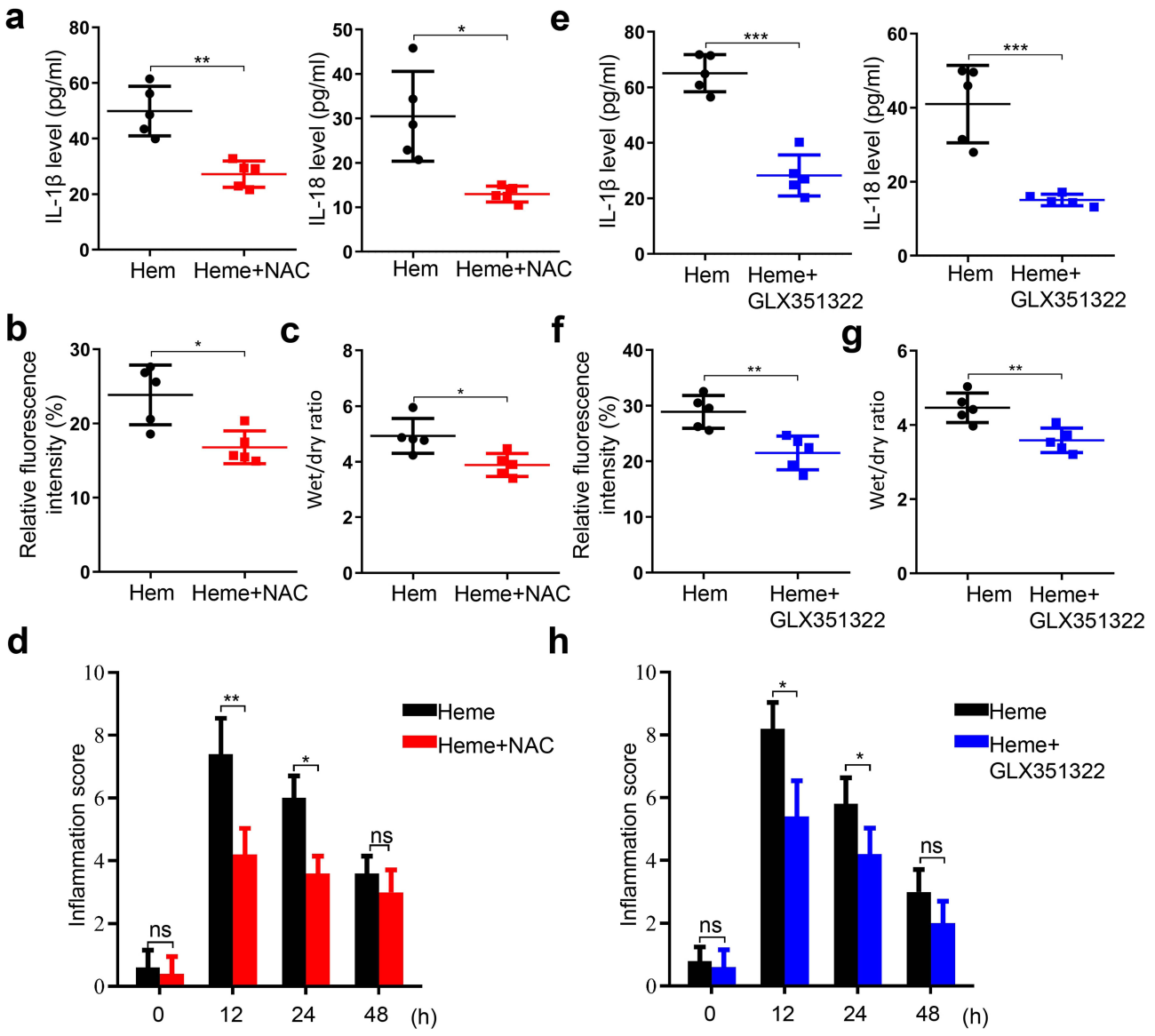

Figure 6 NAC and GLX351322 alleviate heme-inducing SIRS in mice. (**a**) The levels of IL-1β and IL-18 in mice serum were measured after heme and NAC treatment. (**b**) Mice were intravenously injected with tetramethylrhodamine-dextran after heme and NAC treatment at 24 h and the lung vascular permeability was examined by multiphoton-microscope. (**c**) The wet-to-dry lung ratio was calculated after heme and NAC treatment. (**d**) The inflammation score of mice was measured at 0 h, 12 h, 24 h, and 48 h after heme and NAC treatment. (**e**) The levels of IL-1β and IL-18 in mice serum were detected after heme and GLX351322 treatment. (**f**) Mice were intravenously injected with tetramethylrhodamine-dextran after heme and GLX351322 treatment at 24 h and the lung vascular permeability of mice was measured by multi-photon-microscope. (**g**) The wet-to-dry lung ratio was calculated after heme and GLX351322 treatment. (**h**) The inflammation score of mice was measured at 0 h, 12 h, 24 h, and 48 h after heme and GLX351322 treatment. There were 5 mice in each group. The data are expressed as mean ± SEM. ns: no significance, *P < 0.05, **P < 0.01, ***P < 0.001.

permeability and the wet-to-dry lung ratio also decreased in mice after heme and NAC treatment (Figure 6b and c). The inflammation score significantly decreased at 12 and 24h after heme and NAC treatment (Figure 6d). GLX351322, a NOX4 inhibitor, was used to examine this effect. We found that the GLX351322 suppressed the heme-induced increased levels of IL-1β and IL-18 in mice (Figure 6e). Similarly, the vascular permeability, wet-to-dry, and inflammation score decreased after heme and GLX351322 treatment (Figure 6f-h). Collectively, these data indicate that NAC and GLX351322 may reverse heme-inducing SIRS. Next, we treated hemangioma carrying mice with or without GLX351322 after RFA. The serum levels of IL-1β and IL-18 in mice after GLX351322 treatment were significantly decreased (Supplemental Figure 2a). Vascular permeability, the wet-to-dry lung ratio and inflammation score also decreased in mice after GLX351322 treatment (Supplemental Figure 2b-d). Furthermore, GLX351322 inhibited the heme-induced increase in the levels of GSDMD-N and Casp1 p20 in HLMVECs (Supplemental Figure 2e). These data indicate that GLX351322 may reverse SIRS after RFA of hemangioma.

Discussion

In the present study, we found that SIRS occurs in hepatic hemangiomas after RFA and that heme-inducing endothelial cell pyroptosis is involved in this process. These findings provide a new strategy for the prevention of SIRS in patients with hepatic hemangiomas after RFA.

SIRS is defined as the activation of inflammatory, coagulation, innate immune, and repair pathways.[25] Studies have demonstrated that patients with SIRS experience higher rates of morbidity, increased incidence of postoperative morbidity, including cardiovascular complications, and slower recovery of function across both cardiac and non-cardiac surgeries.[26] Our previous study showed that SIRS is a common complication of RFA in hepatic hemangiomas, manifesting as changes in body temperature, heart rate, respiration, and white blood cell count during or shortly after ablation.[5] The incidence and severity of SIRS increase with larger hepatic hemangiomas, and serious complications include acute respiratory distress syndrome and myocardial injury. The incidence rate of SIRS and related complications after RFA for hepatic hemangiomas was 41.6%, which was an important factor affecting the efficacy of hepatic hemangiomas after RFA.[5] In a previous study, we confirmed that SIRS occurred in patients with hepatic hemangiomas after RFA. Furthermore, we simulated SIRS in mice with orthotopic hepatic hemangiomas after RFA.

When hepatic hemangiomas are ablated, a large number of red blood cells are destroyed and hemoglobin is released into the blood. The released hemoglobin is easily oxidized to form methemoglobin and free hemoglobin, which in turn releases heme. Generally, globin- and heme-binding proteins bind to hemoglobin and heme to remove them.[27] However, a large amount of hemoglobin entering the bloodstream within a short period can lead to a relative insufficiency of globin and heme-binding proteins, which in turn leads to the accumulation of hemoglobin and heme in the blood. Our results demonstrated that heme levels significantly increased in hepatic hemangiomas after RFA, indicating that heme may play a key role in SIRS.

Circulating free heme is associated with an increased risk of several hemolytic disorders and correlates with endothelial barrier dysfunction.[28–30] Endothelial cells play a key role in SIRS.[31] DAMP drives endothelial reprogramming to a proinflammatory phenotype, and endothelial cells release cytokines, chemokines, and procoagulant factors and express pro-adhesion molecules, leading to increased permeability of proteins and fluids, resulting in interstitial leakage and SIRS.[32] Heme can induce a rapid decrease in the endothelial barrier integrity of HLMVECs via the MKK3/p38MAPK axis, and is involved in hemolysis-related lung complications.[13] We also found that heme promoted endothelial permeability in vitro and in vivo, which was involved in SIRS.

Pyroptosis is a programmed form of cell death in which cells expand until their membranes rupture, releasing cell contents such as IL-1β and IL-18, which in turn activate inflammation.[33] Endothelial cell pyroptosis is involved in the occurrence and development of related diseases.[34–36] Pyroptosis occurs in neurons, glial cells, and endothelial cells after intracerebral hemorrhage, causing cell death and release of inflammatory factors, leading to a secondary immune-inflammatory response and brain injury.[34] Pyroptosis is a dominant cell death process in cardiomyocytes, immune cells, endothelial cells, and cardiac fibroblasts and participates in the pathogenesis of cardiac diseases that contribute to heart failure.[35] Sinusoidal liver endothelial cells contribute to liver fibrosis through inflammasome activation and pyroptosis.[36] Our results showed that heme-induced endothelial cell pyroptosis occurred through the NLRP3/GSDMD axis, and GSDMD deletion suppressed the effects of heme on SIRS in mice. Therefore, heme-induced pyroptosis is the core of SIRS in hepatic hemangiomas after RFA.

ROS causes oxidative stress responses, leading to cellular dysfunction and pathological changes that play important roles in cancer, inflammation, and neurodegenerative diseases.[37] ROS induces NLPR3 inflammasome formation, leading to endothelial cell pyroptosis.[38,39] In the present study, we found that heme-promoted ROS generation in HLMVECs and NAC inhibited heme-induced SIRS in mice, implying that ROS scavengers may be used to prevent SIRS in hepatic hemangioma after RFA. NOX4 is a member of the nicotinamide adenine dinucleotide phosphate oxidase family that controls oxidative stress.[40,41] Studies have shown that the upregulation of NOX4 expression can lead to an increase in ROS production and plays a key role in mitochondrial dysfunction and apoptosis.[42] In the current study, we found that heme regulates ROS levels through NOX4. NOX4 inhibitors suppress heme-induced SIRS in mice. Furthermore, elevated ROS production causes TXNIP to

dissociate from its inhibitor TRX, leading to NLRP3 inflammasome activation.[43] Therefore, NOX4/ROS/TXNIP-TRX mediates heme-inducing pyroptosis, suggesting that targeted intervention of the molecule in the signaling pathway could suppress SIRS in hepatic hemangiomas after RFA.

Conclusion

We found that SIRS occurred in hepatic hemangiomas after RFA and that heme was involved in this process. Our findings suggest that heme induces endothelial cell pyroptosis and promotes endothelial permeability in HLMVECs through NOX4/ROS/TNXIP-TRX/NLRP3/GSDMD pathways, and decreasing heme level and ROS scavengers may be used to prevent SIRS in hepatic hemangioma after RFA.

Abbreviations

SIRS, Systemic inflammatory response syndrome; RFA, Radiofrequency ablation; HLMVECs, Human lung microvascular endothelial cells; ROS, Reactive oxygen species; NLRP3, Nod-like receptor pyrin domain containing 3; GSDMD, Gasdermin D; NOX4, NADPH oxidase 4; TXNIP, thioredoxin-interacting protein; TRX, thioredoxin family protein.

Data Sharing Statement

All data generated was showed in this manuscript. The datasets used and/or analysed during the current study are available from the corresponding author on reasonable request.

Ethics Statement

All animal experiments conformed to the European Parliament Directive (2010/63/EU) and were approved by the Institutional Animal Care and Use Committee of Beijing Chaoyang Hospital, Capital Medical University and the Ethics committee of Beijing Chaoyang Hospital, Capital Medical University.

Funding

This work was supported by the Beijing Natural Science Foundation (Grant No. 7222069), Beijing Chaoyang Hospital Foundation (Grant No. CYJZ202141) and the Beijing Natural Science Foundation (Grant No. 7212044).

Disclosure

The authors declare that they have no conflicts of interest.

References

1. Ayoobi Yazdi N, Mehrabinejad -M-M, Dashti H, et al. Percutaneous Sclerotherapy with Bleomycin and Ethiodized Oil: a Promising Treatment in Symptomatic Giant Liver Hemangioma. *Radiology*. 2021;301(2):464–471. doi:10.1148/radiol.2021204444
2. Gao J, Fan RF, Yang JY, et al. Radiofrequency ablation for hepatic hemangiomas: a consensus from a Chinese panel of experts. *World J Gastroenterol*. 2017;23(39):7077–7086. doi:10.3748/wjg.v23.i39.7077
3. Maruyama H, Tobari M, Nagamatsu H, et al. Ablation for Benign Liver Tumors: current Concepts and Limitations. *J Clin Transl Hepatol*. 2023;11(1):244–252. doi:10.14218/JCTH.2022.00205
4. Maitra S, Som A, Bhattacharjee S. Accuracy of quick Sequential Organ Failure Assessment (qSOFA) score and systemic inflammatory response syndrome (SIRS) criteria for predicting mortality in hospitalized patients with suspected infection: a meta-analysis of observational studies. *Clin Microbiol Infect*. 2018;24(11):1123–1129. doi:10.1016/j.cmi.2018.03.032
5. Wu S, Gao R, Yin T, et al. Complications of Radiofrequency Ablation for Hepatic Hemangioma: a Multicenter Retrospective Analysis on 291 Cases. *Front Oncol*. 2021;11:706619. doi:10.3389/fonc.2021.706619
6. Yang M, Yang X, Wang S, et al. HMGB1-induced endothelial cell pyroptosis is involved in systemic inflammatory response syndrome following radiofrequency ablation of hepatic hemangiomas. *Am J Transl Res*. 2019;11(12):7555–7567.
7. Salgar S, Bolivar BE, Flanagan JM, et al. The NLRP3 inflammasome fires up heme-induced inflammation in hemolytic conditions. *Transl Res*. 2022. doi:10.1016/j.trsl.2022.08.011
8. Madyaningrana K, Vijayan V, Nikolin C, et al. Alpha1-antitrypsin counteracts heme-induced endothelial cell inflammatory activation, autophagy dysfunction and death. *Redox Biol*. 2021;46:102060. doi:10.1016/j.redox.2021.102060
9. Ryter SW. Significance of Heme and Heme Degradation in the Pathogenesis of Acute Lung and Inflammatory Disorders. *Int J Mol Sci*. 2021;22(11):5509. doi:10.3390/ijms22115509
10. Zhang P, Nguyen J, Abdulla F, et al. Soluble MD-2 and Heme in Sickle Cell Disease Plasma Promote Pro-Inflammatory Signaling in Endothelial Cells. *Front Immunol*. 2021;12:632709. doi:10.3389/fimmu.2021.632709

11. Wu B, Wu Y, Tang W. Heme Catabolic Pathway in Inflammation and Immune Disorders. *Front Pharmacol*. 2019;10:825. doi:10.3389/fphar.2019.00825
12. Erdei J, Toth A, Balogh E, et al. Induction of NLRP3 Inflammasome Activation by Heme in Human Endothelial Cells. *Oxid Med Cell Longev*. 2018;2018:4310816. doi:10.1155/2018/4310816
13. James J, Srivastava A, Varghese MV, et al. Heme induces rapid endothelial barrier dysfunction via the MKK3/p38MAPK axis. *Blood*. 2020;136(6):749–754. doi:10.1182/blood.2019003986
14. Wei X, Xie F, Zhou X, et al. Role of pyroptosis in inflammation and cancer. *Cell Mol Immunol*. 2022;19(9):971–992. doi:10.1038/s41423-022-00905-x
15. Huang C, Li J, Zhang C. What role does pyroptosis play in cancer? *Mol Metab*. 2022;65:101587. doi:10.1016/j.molmet.2022.101587
16. Coll RC, Schroder K, Pelegrin P. NLRP3 and pyroptosis blockers for treating inflammatory diseases. *Trends Pharmacol Sci*. 2022;43(8):653–668. doi:10.1016/j.tips.2022.04.003
17. Wu Y, Pan B, Zhang Z, et al. Caspase-4/11-Mediated Pulmonary Artery Endothelial Cell Pyroptosis Contributes to Pulmonary Arterial Hypertension. *Hypertension*. 2022;79(3):536–548. doi:10.1161/HYPERTENSIONAHA.121.17868
18. Kerr NA, de Rivero Vaccari JP, Umland O, et al. Human Lung Cell Pyroptosis Following Traumatic Brain Injury. *Cells*. 2019;8(1):69. doi:10.3390/cells8010069
19. Jia C, Zhang J, Chen H, et al. Endothelial cell pyroptosis plays an important role in Kawasaki disease via HMGB1/RAGE/cathespin B signaling pathway and NLRP3 inflammasome activation. *Cell Death Dis*. 2019;10(10):778. doi:10.1038/s41419-019-2021-3
20. Wang S, Yang M, Yang X, et al. Endothelial pyroptosis underlies systemic inflammatory response following radiofrequency ablation of hepatic hemangiomas. *Scand J Clin Lab Invest*. 2019;79(8):619–628. doi:10.1080/00365513.2019.1689428
21. Yang X, Liu J, Yang MM, et al. Heme is involved in the systemic inflammatory response following radiofrequency ablation of hepatic hemangiomas. *Eur J Gastroenterol Hepatol*. 2020;32(9):1200–1206. doi:10.1097/MEG.0000000000001636
22. Jeong HG, Cha BG, Kang DW, et al. Ceria Nanoparticles Fabricated with 6-Aminohexanoic Acid that Overcome Systemic Inflammatory Response Syndrome. *Adv Healthc Mater*. 2019;8(9):e1801548. doi:10.1002/adhm.201801548
23. Thomas JJ, Harp KO, Bashi A, et al. MiR-451a and let-7i-5p loaded extracellular vesicles attenuate heme-induced inflammation in hiPSC-derived endothelial cells. *Front Immunol*. 2022;13:1082414. doi:10.3389/fimmu.2022.1082414
24. Reis J, Gorgulla C, Massari M, et al. Targeting ROS production through inhibition of NADPH oxidases. *Nat Chem Biol*. 2023;19(12):1540–1550. doi:10.1038/s41589-023-01457-5
25. Cahill LA, Joughin BA, Kwon WY, et al. Multiplexed Plasma Immune Mediator Signatures Can Differentiate Sepsis From NonInfective SIRS: American Surgical Association 2020 Annual Meeting Paper. *Ann Surg*. 2020;272(4):604–610. doi:10.1097/SLA.0000000000004379
26. Fransvea P, Costa G, Lepre L, et al. Metabolic Syndrome (MetS), Systemic Inflammatory Response Syndrome (SIRS), and Frailty: is There any Room for Good Outcome in the Elderly Undergoing Emergency Surgery? *Front Surg*. 2022;9:870082. doi:10.3389/fsurg.2022.870082
27. Pradhan P, Vijayan V, Gueler F, et al. Interplay of Heme with Macrophages in Homeostasis and Inflammation. *Int J Mol Sci*. 2020;21(3):740. doi:10.3390/ijms21030740
28. Santaterra VAG, Fiusa MML, Hounkpe BW, et al. Endothelial Barrier Integrity Is Disrupted In Vitro by Heme and by Serum From Sickle Cell Disease Patients. *Front Immunol*. 2020;11:535147. doi:10.3389/fimmu.2020.535147
29. Gbotosho OT, Kapetanaki MG, Kato GJ. The Worst Things in Life are Free: the Role of Free Heme in Sickle Cell Disease. *Front Immunol*. 2020;11:561917. doi:10.3389/fimmu.2020.561917
30. Gonzales J, Holbert K, Czysz K, et al. Hemin-Induced Endothelial Dysfunction and Endothelial to Mesenchymal Transition in the Pathogenesis of Pulmonary Hypertension Due to Chronic Hemolysis. *Int J Mol Sci*. 2022;23(9):4763. doi:10.3390/ijms23094763
31. Molema G, Zijlstra JG, van Meurs M, et al. Renal microvascular endothelial cell responses in sepsis-induced acute kidney injury. *Nat Rev Nephrol*. 2022;18(2):95–112. doi:10.1038/s41581-021-00489-1
32. Serna-Rodriguez MF, Bernal-Vega S, de la Barquera JAO, et al. The role of damage associated molecular pattern molecules (DAMPs) and permeability of the blood-brain barrier in depression and neuroinflammation. *J Neuroimmunol*. 2022;371:577951. doi:10.1016/j.jneuroim.2022.577951
33. Pan Y, Cai W, Huang J, et al. Pyroptosis in development, inflammation and disease. *Front Immunol*. 2022;13:991044. doi:10.3389/fimmu.2022.991044
34. Song D, Yeh CT, Wang J, et al. Perspectives on the mechanism of pyroptosis after intracerebral hemorrhage. *Front Immunol*. 2022;13:989503. doi:10.3389/fimmu.2022.989503
35. Habimana O, Modupe Salami O, Peng J, et al. Therapeutic implications of targeting pyroptosis in Cardiac-related etiology of heart failure. *Biochem Pharmacol*. 2022;204:115235. doi:10.1016/j.bcp.2022.115235
36. Gan C, Cai Q, Tang C, et al. Inflammasomes and Pyroptosis of Liver Cells in Liver Fibrosis. *Front Immunol*. 2022;13:896473. doi:10.3389/fimmu.2022.896473
37. Wang P, Gong Q, Hu J, et al. Reactive Oxygen Species (ROS)-Responsive Prodrugs, Probes, and Theranostic Prodrugs: applications in the ROS-Related Diseases. *J Med Chem*. 2021;64(1):298–325. doi:10.1021/acs.jmedchem.0c01704
38. Liu X, Li M, Chen Z, et al. Mitochondrial calpain-1 activates NLRP3 inflammasome by cleaving ATP5A1 and inducing mitochondrial ROS in CVB3-induced myocarditis. *Basic Res Cardiol*. 2022;117(1):40. doi:10.1007/s00395-022-00948-1
39. Liu M, Lu J, Chen Y, et al. Sodium Sulfite-Induced Mast Cell Pyroptosis and Degranulation. *J Agric Food Chem*. 2021;69(27):7755–7764.
40. Matuz-Mares D, Vazquez-Meza H, Vilchis-Landeros MM. NOX as a Therapeutic Target in Liver Disease. *Antioxidants*. 2022;11(10):2038. doi:10.3390/antiox11102038
41. Nabeebaccus AA, Reumiller CM, Shen J, et al. The regulation of cardiac intermediary metabolism by NADPH oxidases. *Cardiovasc Res*. 2023;118(17):3305–3319. doi:10.1093/cvr/cvac030
42. Vermot A, Petit-Hartlein I, Smith SME, et al. NADPH Oxidases (NOX): an Overview from Discovery, Molecular Mechanisms to Physiology and Pathology. *Antioxidants*. 2021;10(6):890. doi:10.3390/antiox10060890
43. Tschopp J, Schroder K. NLRP3 inflammasome activation: the convergence of multiple signalling pathways on ROS production? *Nat Rev Immunol*. 2010;10(3):210–215. doi:10.1038/nri2725

Journal of Inflammation Research

Dovepress

Publish your work in this journal

The Journal of Inflammation Research is an international, peer-reviewed open-access journal that welcomes laboratory and clinical findings on the molecular basis, cell biology and pharmacology of inflammation including original research, reviews, symposium reports, hypothesis formation and commentaries on: acute/chronic inflammation; mediators of inflammation; cellular processes; molecular mechanisms; pharmacology and novel anti-inflammatory drugs; clinical conditions involving inflammation. The manuscript management system is completely online and includes a very quick and fair peer-review system. Visit http://www.dovepress.com/testimonials.php to read real quotes from published authors.

Submit your manuscript here: https://www.dovepress.com/journal-of-inflammation-research-journal